The Climatology, Meteorology, and Boundary Layer Structure of Marine Cold Air Outbreaks in Both Hemispheres*

JENNIFER FLETCHER, SHANNON MASON, AND CHRISTIAN JAKOB

School of Earth, Atmosphere, and Environment, Monash University, Clayton, Victoria, Australia

(Manuscript received 16 April 2015, in final form 25 September 2015)

ABSTRACT

A comparison of marine cold air outbreaks (MCAOs) in the Northern and Southern Hemispheres is presented, with attention to their seasonality, frequency of occurrence, and strength as measured by a cold air outbreak index. When considered on a gridpoint-by-gridpoint basis, MCAOs are more severe and more frequent in the Northern Hemisphere (NH) than the Southern Hemisphere (SH) in winter. However, when MCAOs are viewed as individual events regardless of horizontal extent, they occur more frequently in the SH. This is fundamentally because NH MCAOs are larger and stronger than those in the SH. MCAOs occur throughout the year, but in warm seasons and in the SH they are smaller and weaker than in cold seasons and in the NH. In both hemispheres, strong MCAOs occupy the cold air sector of midlatitude cyclones, which generally appear to be in their growth phase. Weak MCAOs in the SH occur under generally zonal flow with a slight northward component associated with weak zonal pressure gradients, while weak NH MCAOs occur under such a wide range of conditions that no characteristic synoptic pattern emerges from compositing. Strong boundary layer deepening, warming, and moistening occur as a result of the surface heat fluxes within MCAOs.

1. Introduction

Marine cold air outbreaks (MCAOs) are high-impact weather events in which air masses of polar or cold continental origin are advected over relatively warm open ocean. The resulting instability can lead to strong boundary layer turbulence and surface heat loss from the ocean (Brümmer 1996), as well as severe weather such as polar lows and boundary layer fronts (Businger 1985; Carleton and Song 1997; Rasmussen and Turner 2003).

During MCAOs the air–sea temperature difference is particularly strong. The resulting intense heat loss from the sea surface to the atmosphere in MCAOs suggests that they play a role in high-latitude ocean–atmosphere heat exchange, including in regions of deep-water formation (Condron et al. 2008; Isachsen et al. 2013). Their role in ocean–atmosphere heat exchange is disproportionate to their frequency of occurrence, and in the Southern Ocean Pacific sector they dominate seasonal extremes in surface sensible heat flux (SHF; Papritz et al. 2015).

Intense cold air outbreaks are associated with roll convection leading to organized cellular convection downstream (Etling and Brown 1993; Atkinson and Wu Zhang 1996). These have been studied in the Northern Hemisphere (NH) through remote sensing (Brümmer and Pohlmann 2000), in situ observations (Hein and Brown 1988; Chou and Ferguson 1991; Brümmer 1999; Renfrew and Moore 1999), and modeling studies (Stage and Businger 1981; Müller and Chlond 1996; Schröter et al. 2005). An extensive body of knowledge on the relationship between meteorology and clouds in these environments now exists based on these studies.

General circulation models tend to simulate both Northern Hemisphere MCAOs and Southern Hemisphere midlatitude cyclones in general with too little stratiform cloud cover (Field et al. 2014; Williams et al. 2013; Bodas-Salcedo et al. 2014). For this reason, field

---

experiments on NH MCAOs have been used for climate model evaluation and development (Bodas-Salcedo et al. 2012). This is particularly the case in attempts to reduce the Southern Hemisphere (SH) radiation bias (Trenberth and Fasullo 2010), in which most models' Southern Ocean clouds do not reflect enough shortwave radiation, leading to too-warm sea surface temperatures and affecting the entire SH energy budget (Hwang and Frierson 2013). If one assumes that some of this bias in climate models is due to cold air outbreaks, case studies of NH MCAOs can be used to test model changes aimed at reducing biases in Southern Ocean clouds. Such work has proven useful for this goal (Bodas-Salcedo et al. 2012); nonetheless, it remains unknown how similar Northern Hemisphere MCAOs are to those in the Southern Hemisphere.

There have already been several studies of SH MCAOs. These first required a definition of an MCAO, and all used variations on that of Kolstad and Bracegirdle (2008), who proposed an MCAO index suitable for coarse-resolution datasets such as reanalysis or climate models. This index was based on the potential temperature difference between the surface and 700 hPa, divided by the pressure difference between 700 hPa and sea level. The 700-hPa pressure level was chosen primarily based on what was available from reanalysis at the time.

Previous studies of SH MCAOs used variations on this index, some using 700-hPa geopotential height instead of the 700 hPa–sea level pressure difference (Bracegirdle and Kolstad 2010). More recently, Papritz et al. (2015) used the 850-hPa to surface potential temperature difference to define the MCAO index. They showed that this index was a good predictor of the surface sensible heat flux for the Ross and Amundsen–Bellingshausen Seas. In this sense it is well suited to the study of cold air outbreaks, as opposed to polar low formation, which may be better captured by the static stability measures used by Kolstad and Bracegirdle (2008) and Bracegirdle and Kolstad (2010).

Bracegirdle and Kolstad (2010) found that daily and monthly variability in Southern Ocean MCAOs was largely associated with lower-tropospheric temperature variability, while on seasonal time scales it was also due to sea surface temperature (SST) variability. They also found that wintertime interannual variability in MCAOs was associated with the southern annular mode (SAM) in high-latitude ice-free regions, but not in the midlatitudes. This likely reflects the greater availability of storms to transport air overlying sea ice to open ocean under positive SAM conditions, as well as the correlation between SAM and sea ice extent, the latter of which

determines the availability of cold air masses at Southern high latitudes (Simpkins et al. 2012).

Kolstad (2011) used an MCAO index along with the dynamic tropopause pressure to define regions throughout the globe favorable for polar low development. The MCAO index generally limited where polar lows could form, with most SH polar lows forming in the Pacific sector. Monthly variability in the MCAO index largely determined the frequency of occurrence of polar lows.

Papritz et al. (2015) used an MCAO index to show that wintertime SH Pacific sector MCAOs were largely associated with extratropical cyclones and with air masses that are advected off of sea ice or the Antarctic continent. They also showed that MCAOs' contribution to wintertime surface heat fluxes is disproportionate to their frequency of occurrence.

In this paper, we build on previous work in order to deepen the understanding of Southern Hemisphere MCAOs, their similarities to and differences from their Northern Hemisphere counterparts, their seasonal variability, and their synoptic environment. We use an MCAO index similar to those used in the above studies and confirm that its seasonality and interhemispheric contrasts are consistent with previous results. We add to those previous studies by using the MCAO index to identify individual MCAO events and to study their composite thermodynamic and dynamic structure.

This paper is organized as follows: section 2 describes the data used, defines the MCAO index, and presents the climatological features of that index. Section 3 defines MCAO events and shows their synoptic environment. Section 4 summarizes the results and indicates future work motivated by this study.

2. The climatology of MCAOs

a. Data description

We used output from the European Centre for Medium-Range Weather Forecasts (ECMWF) interim reanalysis (ERA-Interim; Dee et al. 2011; http://apps.ecmwf.int/datasets/data/interim-full-daily/levtype=sfc/): twice-daily analysis, at 0000 and 1200 UTC, from September 1979 to August 2014. The data are on a 1° equally spaced latitude–longitude grid. We also used ERA-Interim twice-daily 12-h forecasts of surface sensible heat flux at 0000 and 1200 UTC. All variables are instantaneous except fluxes, which are averages over the 12 hours following the instantaneous data.

b. MCAO index definition

We defined an MCAO index as $M = \theta_{\text{SKT}} - \theta_{800}$ (i.e., the potential temperature difference between the
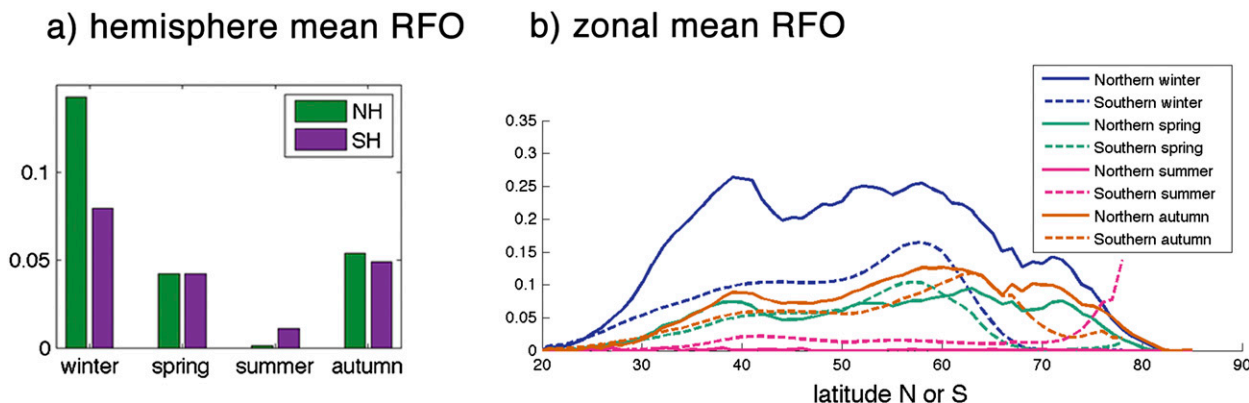
FIG. 1. Gridpoint-by-gridpoint area-weighted RFO of $M > 0$ by (a) hemisphere and (b) zonal mean.

surface skin and 800 hPa). Using the surface skin temperature rather than SST prevents spurious MCAO diagnosis in areas of high sea ice cover. Positive M defines an absolutely unstable lower troposphere and was our bare minimum to define a cold air outbreak (Kolstad et al. 2009).

Our MCAO index (i.e., M) is similar to indices used in other work on cold air outbreaks in the Southern and Northern Hemispheres, with slight differences in definition producing quantitative differences in the index but qualitative similarities in its global structure. For example, Kolstad et al. (2009) and subsequent work (Bracegirdle and Kolstad 2010; Kolstad 2011) used the potential temperature at 700 hPa, while Papritz et al. (2015) used 850-hPa potential temperature. We tested all of these indices and found that using the 800-hPa level produced more high-latitude MCAOs than using the 700-hPa level, while using 850 hPa produced a similar climatology to 800 hPa at middle and high latitudes but identified more MCAOs in the subtropics (not shown).

To give the reader a greater intuition for what the MCAO index captures, we include as supplemental material a 1-yr animation of the twice-daily M in the extratropics. To emphasize MCAO events, we excluded values of $M \leq 0$.

c. Climatology of the MCAO index

Figure 1 shows the seasonal relative frequency of occurrence (RFO) with which grid points have $M > 0$ for area-weighted hemispheric (poleward of 20°) means (Fig. 1a) and zonal means (Fig. 1b). The relative frequency was determined by dividing the number of hits of $M > 0$ by the number of opportunities; that is, the number of oceanic grid points in a hemisphere or latitude band over the length of the time series. Seasons were defined as follows: winter is December–February

(DJF) in the NH and June–August (JJA) in the SH; spring is March–May (MAM) in the NH and September–November (SON) in the SH, and so forth.

Figure 1 shows that M is greater than zero most often in winter in both hemispheres, but it also shows that this occurs almost as often in shoulder seasons as it does in winter, particularly in the Southern Hemisphere. The NH annual cycle in M is much greater than that of the SH.

There is an apparent discrepancy between Figs. 1a and 1b: while Fig. 1a shows both hemispheres having similar RFO in spring and autumn, Fig. 1b generally shows the RFO being greater in the NH during those two seasons. This is because the RFO is calculated with respect to the number of grid points available for an MCAO (i.e., oceanic grid points). In the midlatitudes, the NH has far fewer of these than the SH, while the opposite is true at high latitudes. This means that the NH-average RFO places less weight on the midlatitude grid points than would appear from Fig. 1b, while the SH-average RFO places less weight on the high-latitude grid points. Both of these act to increase the hemisphere-mean RFO in the SH relative to the NH.

Figure 1b also shows that at SH high latitudes, the MCAO index is greater than zero more often in autumn than in winter. This is because in winter the high latitudes have extensive sea ice cover and, therefore, low surface skin temperature, reducing the MCAO index. Papritz et al. (2015) showed that in the South Pacific, the maximum in MCAO frequency closely followed the sea ice edge with each season.

Figure 2 shows the wintertime RFO of all MCAOs and the magnitude of very strong MCAOs (i.e., the 95th percentile of the index). Figures 2a and 2b show that in both hemispheres $M > 0$ most often in regions downstream of cold continents or areas of high sea ice cover, as well as midlatitude regions with a strong SST gradient,

M > 0 relative frequency of occurrence
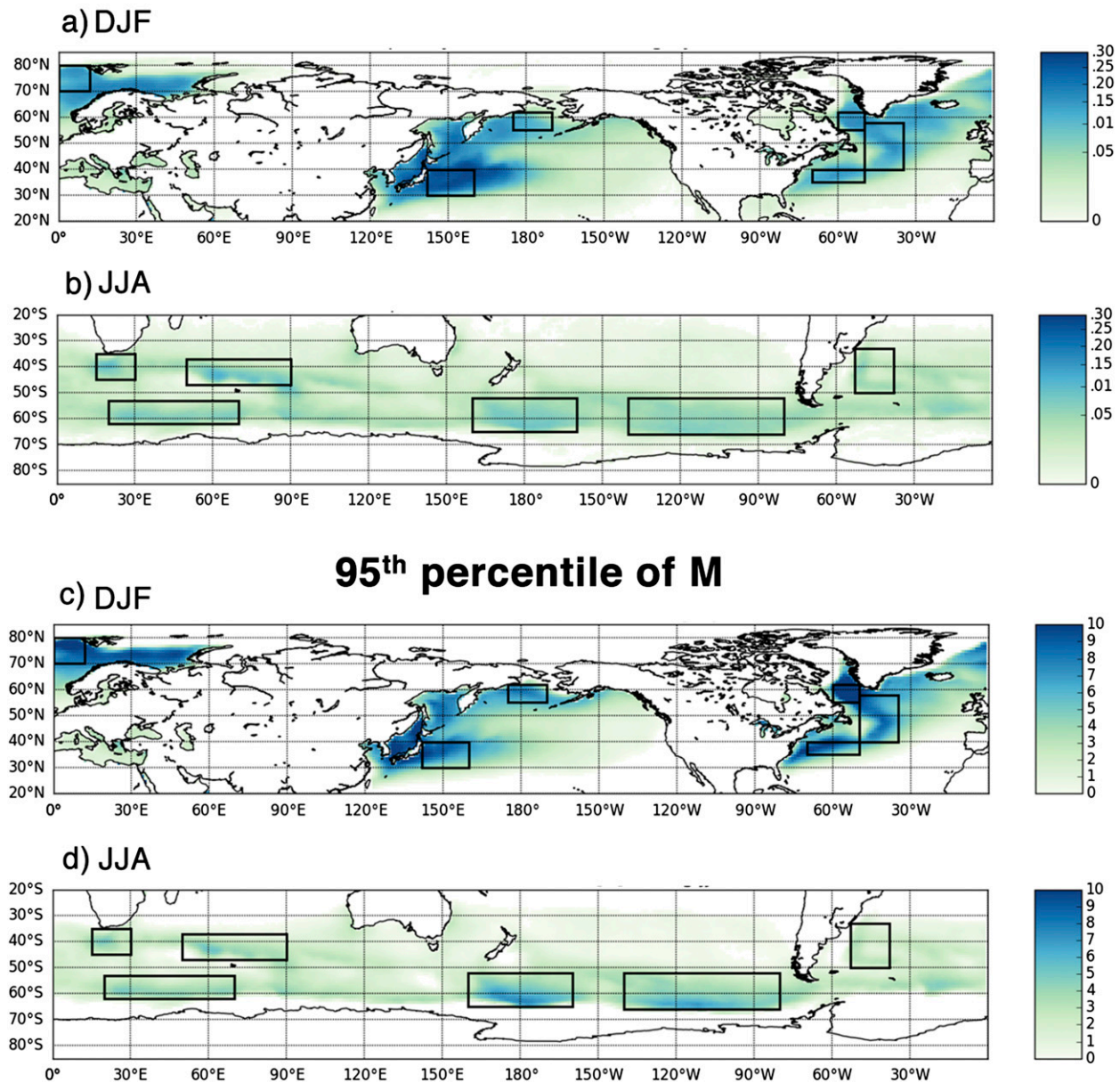

95th percentile of M

FIG. 2. Wintertime $M > 0$ RFO in the (a) NH and (b) SH. The scale in (a) and (b) is quadratic to allow easier comparison between hemispheres. The 95th percentile of M in wintertime in the (c) NH and (d) SH. Black boxes show the following regions used in composites in section 3, ordered from west to east, for the NH: the Norwegian Sea, the Kuroshio, the Bering Sea, the Gulf Stream, the Labrador Sea, and the North Atlantic; and for the SH: the Agulhas Current, the Indian polar front, the Indian subtropical front, the north Ross Sea, the north Bellingshausen Sea, and the Brazil Current.

most notably the Gulf Stream and Kuroshio but also the southern Brazil Current, the Agulhas Current near South Africa, and the Indian Ocean subtropical front.

The differences between the two hemispheres are even more apparent when the strongest 5% of MCAOs are compared, as in Figs. 2c and 2d. Northern Hemisphere MCAOs are not only more frequent but also much stronger than those in the Southern Hemisphere. Figure 2d also highlights the Pacific sector as the main area where strong MCAOs occur in the SH. These results are consistent with those of Bracegirdle and Kolstad (2010) and Kolstad (2011).

Comparing Figs. 2b and 2d, we see that MCAOs occur about as frequently in the Indian Ocean sector of the Southern Ocean as they do in the Pacific sector, but they are weaker in the former than the latter. The local RFO maximum in the high-latitude Indian Ocean sector coincides with regions of maximum extratropical cyclone frequency (Simmonds et al. 2003). As these storms move poleward (Hoskins and Hodges 2005) they advect very cold air masses, often originating over sea ice, equatorward. In the Pacific sector, the Antarctic topography, with the Ross and Amundsen Seas and associated ice shelves, particularly the Ross Ice Shelf corridor (Parish and Bromwich 2007) and the very large area of sea ice over the Ross Sea, provides the most favorable conditions for equatorward advection of polar air masses.

3. The horizontal and vertical structure of MCAO events

a. MCAO event definition and size distribution

Having established some of the climatological features of our MCAO index, we used this index to define MCAO events, to study the horizontal and vertical structure of typical MCAO events, and to compare events between different regions, in particular the two hemispheres. We defined an MCAO event as an instantaneous closed contour encircling regions with $M > 0$; events that occupy fewer than eight grid points are excluded. Our results were not sensitive to the eight-gridpoint choice, as the vast majority of MCAOs are much larger than this.

We defined the strength of the event by M_{max}, the maximum value of M within the closed contour. Weak events have $0 < M_{max} \leq 3\,K$, moderate events have $3 < M_{max} \leq 6\,K$, and strong events have $M_{max} > 6\,K$. This range of strengths distinguishes weak events, which can occur year-round, from strong events, which occur mostly in winter. The particular numbers were chosen such that the total number of SH events decreases with each successive category. Category choices are further discussed in section 3b.

As previously mentioned, Fig. 2 implies that some MCAOs are associated with advection of polar air masses over high-latitude oceans, while others involve the advection of continental or cold marine air over SST gradients associated with western boundary currents. This distinction applies more in the NH than in the SH. In the former, MCAO events appear to be mostly stationary or to travel eastward and die out over the open ocean. In the latter, an MCAO originating at high latitudes often travels northward and becomes a midlatitude event (e.g., see supplemental material).
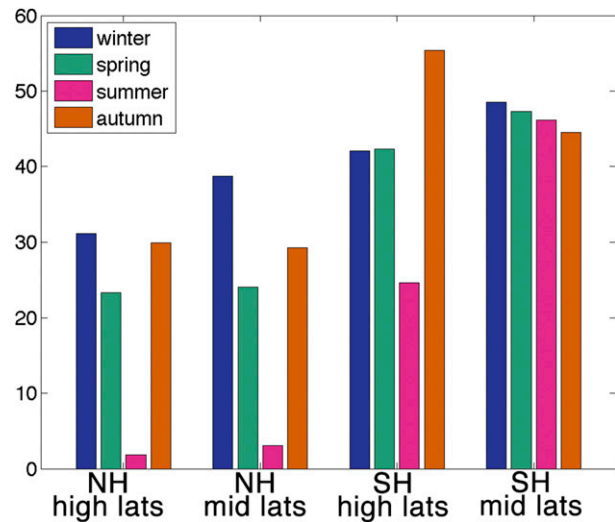

FIG. 3. Number of MCAO events per season, per latitude band. Events are defined from instantaneous snapshots; multiple events defined here may constitute a single, multiday cold air outbreak episode.

To account for the different origins of high- and midlatitude MCAOs, we further divided MCAO events into those existing between 35° and 55°N/S (midlatitude events) and those existing between 55° and 75°N/S (high-latitude events). Events that overlapped were classified by the location of the maximum in the MCAO index.

Figure 3 shows the number of MCAO events per season and latitude band, comparing the Northern and Southern Hemispheres as well as middle and high latitudes. Because events were counted at single instances in time, the same "weather event" contains multiple MCAO events by our counting; this should be kept in mind when considering raw numbers of events. Since the data are twice daily, if we assume that an event typically lasts around 3 days, then a count of 60 per season corresponds to roughly 10 independent cold air outbreaks.

Figure 3 shows that when MCAOs are viewed as events, rather than on a gridpoint-by-gridpoint basis as in section 2c, they are more frequent in the Southern than in the Northern Hemisphere. There are two plausible, mutually independent reasons for this: MCAOs are smaller in the SH and so occupy fewer grid points, and the greater ocean coverage in the SH provides more opportunities for separate MCAO events. The latter is certainly true; to investigate the former we will explore the sizes of MCAO events.

All latitude belts in Fig. 3 show a weaker annual cycle than that shown in Fig. 1, implying that in warmer seasons MCAOs are smaller and so occupy fewer grid points than in colder seasons. There is almost no annual cycle in the number of events in the SH midlatitudes. Figure 1b shows that this is also the case on a

gridpoint-by-gridpoint basis outside of summer. However, analysis of the seasonality of MCAO strength and event size (not shown) indicated that summertime MCAOs in the SH midlatitudes are small and weak. The weak annual cycle in sea surface temperatures in the Southern Ocean (Trenberth 1991) also likely plays a role. This further suggests that weaker MCAOs are smaller than stronger ones no matter when or where they occur.

To investigate the size of MCAOs, we defined a zonal (meridional) length scale for all events: the maximum length of the closed contour in the east–west (north–south) direction. We used the zonal length scale to define their size. We defined their orientation by their aspect ratio: the ratio of zonal length scale to meridional length scale.

We hypothesized that the size and/or orientation of MCAO events may vary according to (i) location, (ii) season, and (iii) strength. We found that the strength of MCAO events is most related to their size, with stronger events being much larger than weaker ones, as is shown in Fig. 4 (top). However, for the same strength category, SH events are generally larger than NH events, with the exception of strong events in the NH midlatitudes. Nevertheless, because NH MCAOs are stronger on average than SH MCAOs, on the whole MCAOs are larger in the NH. Ultimately, the discrepancy in MCAO frequency between a local, gridpoint view and an event view, particularly in winter, is due to NH MCAOs being stronger and larger. We found that the seasonality of event sizes is largely explained by the seasonality of their strength (not shown).

In section 3b, we will show that MCAOs are associated with midlatitude cyclones, and the size and shape of MCAOs are set primarily by this synoptic-scale meteorology as well as the amplitude and orientation of the surface temperature gradient. Northern Hemisphere high-latitude MCAOs are smaller than their midlatitude counterparts because their size is limited by the ocean basins they tend to occur in (e.g., the Labrador or Norwegian Seas, see Fig. 2). It is likely that if we chose 50° instead of 55° to separate middle and high latitudes, we would find less difference in NH MCAO sizes between the two latitude bands.

Figure 4 (bottom) shows the aspect ratio of MCAOs. Most events have similar zonal and meridional scales. However, SH high-latitude events have a larger zonal than meridional length scale because they occur along a temperature gradient that is mainly north–south. Northern Hemisphere midlatitude events occur on temperature gradients with both north–south and east–west components (mainly the tilted Gulf Stream and Kuroshio), making them less zonally elongated than

Southern Hemisphere high-latitude events. In the NH high latitudes, basin sizes and geometries generally result in MCAO events that are somewhat longer meridionally than zonally.

b. Composite meteorology of MCAOs

To study the synoptic conditions of MCAOs, we composited meteorological quantities on similar events. To be considered similar, events had to be of the same classification of strength and they have to be roughly the same size. Events were selected by size according to the strength category being composited based on Fig. 4. Weak events were included in their composite if they had both zonal and meridional length scales between 450 and 650 km; strong events were included in their composite if they had length scales between 1500 and 2500 km. Intermediate strength events are not shown, but were more similar to strong events than weak ones.

Additionally, we required composited events to be in the same geographical region, as different geometries of surface temperature gradient lead to a different large-scale flow pattern most conducive to lower-tropospheric cold advection (this applies mainly in the NH high latitudes but was used globally). Composites were performed in six regions of both the Northern Hemisphere: the Bering Sea, the Norwegian Sea, the Labrador Sea, the Kuroshio, the Gulf Stream, and the North Atlantic; and the SH: the Indian polar front, the north Ross Sea, the north Bellingshausen Sea, the Indian subtropical front, the Brazil Current, and the Agulhas Current. The locations of these regions are shown in Fig. 2.

Figure 5 shows the distribution of MCAO event strength within each region, expressed as cumulative probabilities. The Kuroshio and Gulf Stream are most likely to have very strong MCAOs. The first tercile (cumulative probability less than 0.33) of event strength ranges from $M_{max} \lesssim 2\,\mathrm{K}$ in most SH regions and some NH regions to $M_{max} \lesssim 7\,\mathrm{K}$ in the Kuroshio region. The third tercile (cumulative probability greater than 0.67) ranges from $M_{max} \gtrsim 4\,\mathrm{K}$ over the Brazil Current to $M_{max} \gtrsim 8\,\mathrm{K}$ for the Gulf Stream. Our choice of strength categories for compositing, with weak corresponding to $M_{max} \lesssim 3\,\mathrm{K}$ and strong corresponding to $M_{max} > 6\,\mathrm{K}$, are in keeping with these results, but the weak category is slightly overrepresented and the strong category is slightly underrepresented.

We computed composites separately for all seasons, but found little difference in the composites between seasons that was not attributable to MCAO strength (e.g., strong events in spring were similar to strong events in winter, but occurred less often). Therefore, in the interest of space, we show results for winter only.
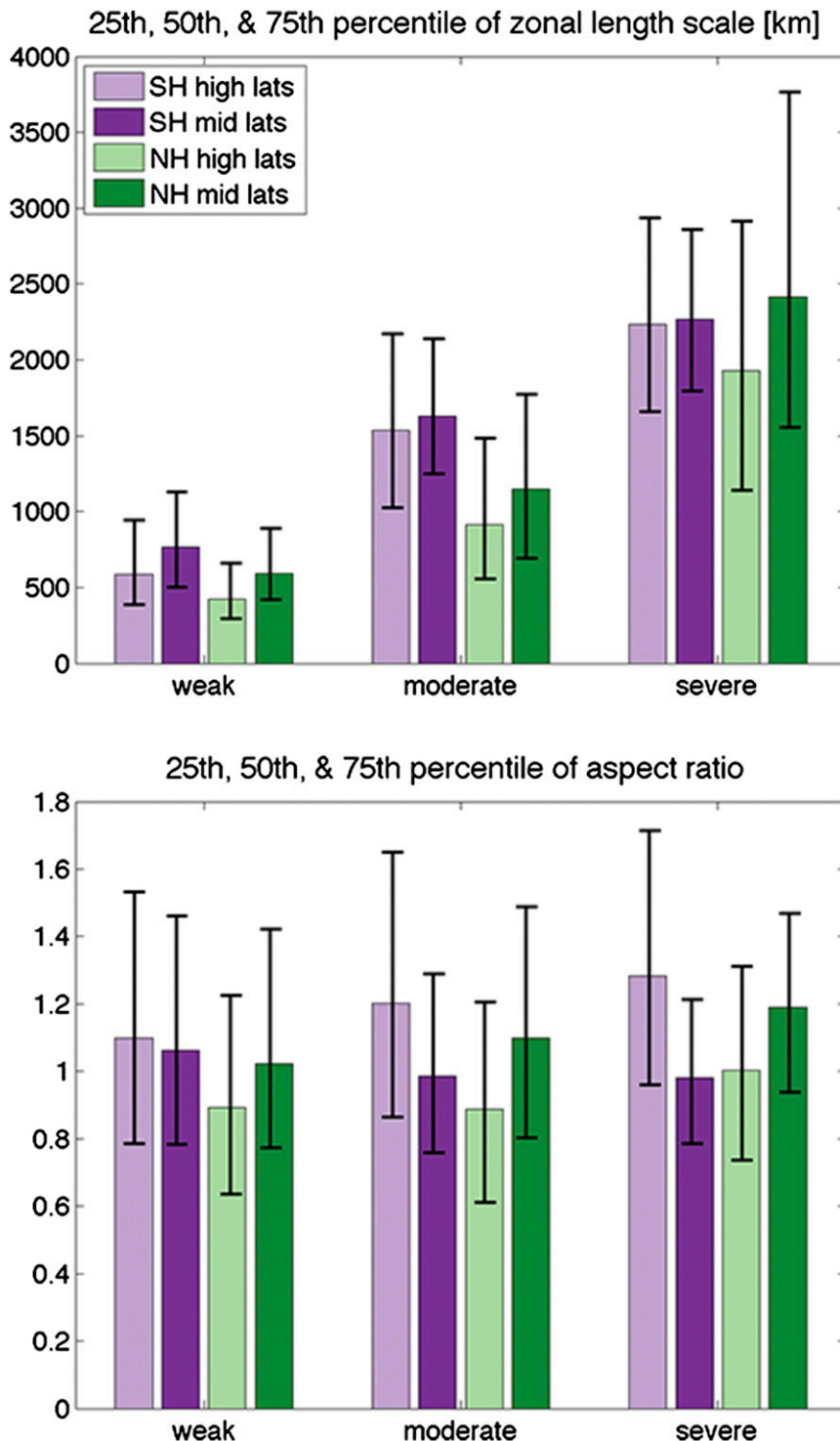
FIG. 4. Size and shape of MCAO events according to location and strength: (top) zonal length scale and (bottom) aspect ratio. The length of the colored bars indicates the 50th percentile of the data, while the black bars show the 25th and 75th percentiles.
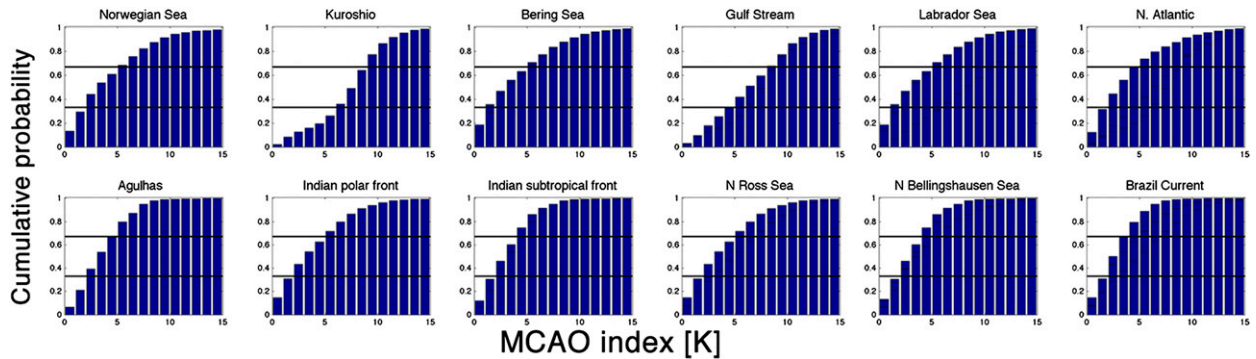
FIG. 5. Cumulative probability of MCAO events having a strength characterized by the M_{max} within the event. Probabilities are shown for each region in which compositing is performed. Black lines indicate the first and third terciles. Probabilities are calculated for DJF in the NH and JJA in the SH. Regions are arranged from west to east starting at the prime meridian, with (top) NH and (bottom) SH.

Prior to compositing, each event was interpolated to a 4000 km × 2000 km grid, with 100-km grid spacing, using nearest-neighbor interpolation. This grid was centered on the location of M_{max} within the closed contour of each event; this point is the origin in figures below.

1) SURFACE PRESSURE, WINDS, AND HEAT FLUXES

Figure 6 shows the composited sea level pressure, 10-m horizontal winds, sea ice cover, and surface sensible heat flux surrounding the MCAO. Within each hemisphere and latitude belt, results were similar across different ocean basins, so we only show three example regions per hemisphere: two high latitude and one midlatitude. Composites for the remaining regions are available as supplemental material. For each hemispheric section of the figure, the top row (Figs. 6a–c, 6j–l) corresponds to 24 h prior to the event, the middle row (Figs. 6d–f, 6m–o) is at the time of the event, and the bottom row (Figs. 6g–i, 6p–q) is 24 h later. The center of the composite is always defined by M_{max} at $t = 0$.

Unsurprisingly, we find that globally MCAOs are associated with the cold air sector of midlatitude cyclones, as was also found by Kolstad et al. (2009) for the North Atlantic and Papritz et al. (2015) for the South Pacific. This result is unsurprising because we expect MCAOs to be associated with equatorward flow, which would generally require low pressure to the east and high pressure to the west, though these pressure anomalies will not necessarily extend to the surface. In both hemispheres, high-latitude events are near well-developed closed surface lows, with winds optimal for cold air advection.
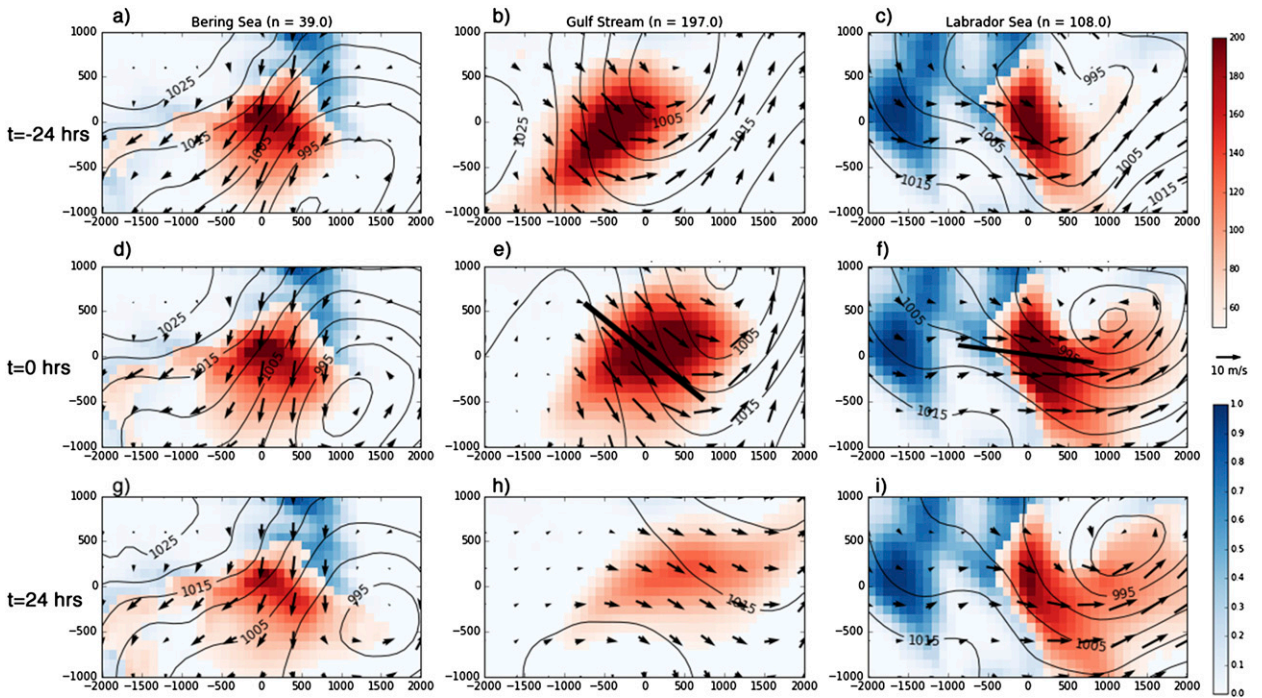
For comparison, Fig. 7 shows the same composites, but for weak MCAO events. Weak events are associated with much weaker or nonexistent surface lows. The NH weak events have light surface winds, well under $10 \, \mathrm{m \, s^{-1}}$, and in the midlatitudes have no characteristic

synoptic signature. These likely represent a mix of cyclones in various stages of growth or decay, and may also include large-scale flow around a weak low that is not part of an extratropical cyclone [Papritz et al. (2015) found that roughly 25% of Pacific sector Southern Ocean MCAOs were not associated with midlatitude cyclones, and weak events are likely to be overrepresented in this category].

Figures 6 and 7 also show composite surface SHF and sea ice cover. Only SHF values greater than $50 \, \mathrm{W \, m^{-2}}$ are shown; this lower threshold is near or above the 95th percentile of high-latitude Southern Ocean SHF for a range of data products (Bourassa et al. 2013). Average SHF ranges from at least $200 \, \mathrm{W \, m^{-2}}$ at the center of strong events to 50–$100 \, \mathrm{W \, m^{-2}}$ in weak events and downwind of strong ones. Figures 6d and 6f illustrate the importance of topography on the specific synoptic environments facilitating MCAO growth in different regions. The strongest MCAOs occur in the Bering Sea region when the large-scale flow is northerly directly through the Bering Strait. In the Labrador Sea (Fig. 6f), the land surface also likely plays a role. Figure 6f shows two regions of high sea ice cover, one about 2000–2500 km west of the surface low and another about 1000 km west of it (partially obscured by the SHF field). These two maxima are an artifact of compositing and do not represent the actual sea ice field. On average the wintertime sea ice edge in the western Labrador Sea is roughly 1000 km west of Cape Farewell, the southern tip of Greenland. This suggests that the surface low tends to be either south of Greenland or to the lee of it. It is likely that Greenland orography plays an important role in the development of the surface cyclones associated with the MCAOs, as it has been shown, for example, in the development of westerly tip jets (Våge et al. 2009).

Figures 6 and 7 also show the time development of the composites. Over the 48-h period of most of the composites, we see the general eastward translation of the
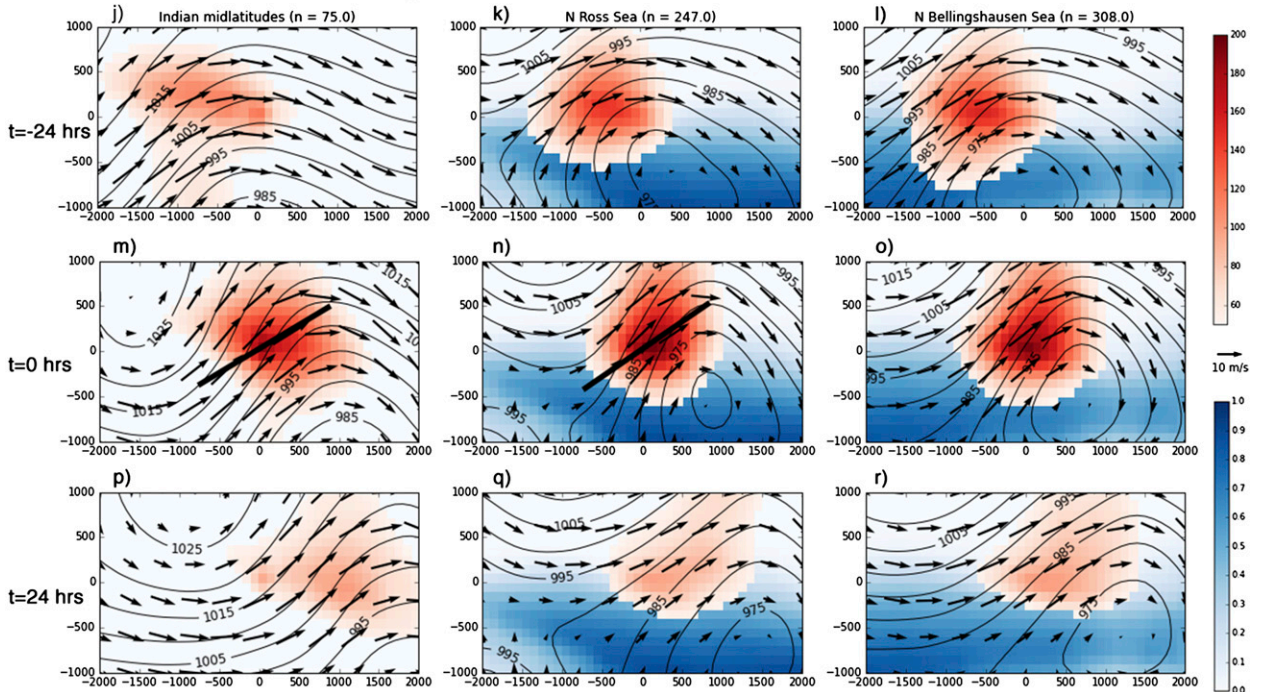
FIG. 6. Composite sea level pressure (hPa; contours), 10-m winds (arrows), fractional sea ice cover (blue), and surface SHF (W m^{-2}; red) for strong ($M_{max} > 6$ K) MCAO events. NH regions: (a),(d),(g) Bering Sea; (b),(e),(h) Gulf Stream; and (c),(f),(i) Labrador Sea. SH regions: (j),(m),(p) Indian Ocean midlatitudes; (k),(n),(q) Ross Sea; and (l),(o),(r) Bellingshausen Sea. Results are 24 h before the MCAO event in (a)–(c) and (j)–(l), at the event time in (d)–(f) and (m)–(o), and 24 h later in (g)–(i) and (p)–(r). Composites are centered on the location of M_{max}. (Solid black lines show schematic locations of cross sections used in Fig. 10.)
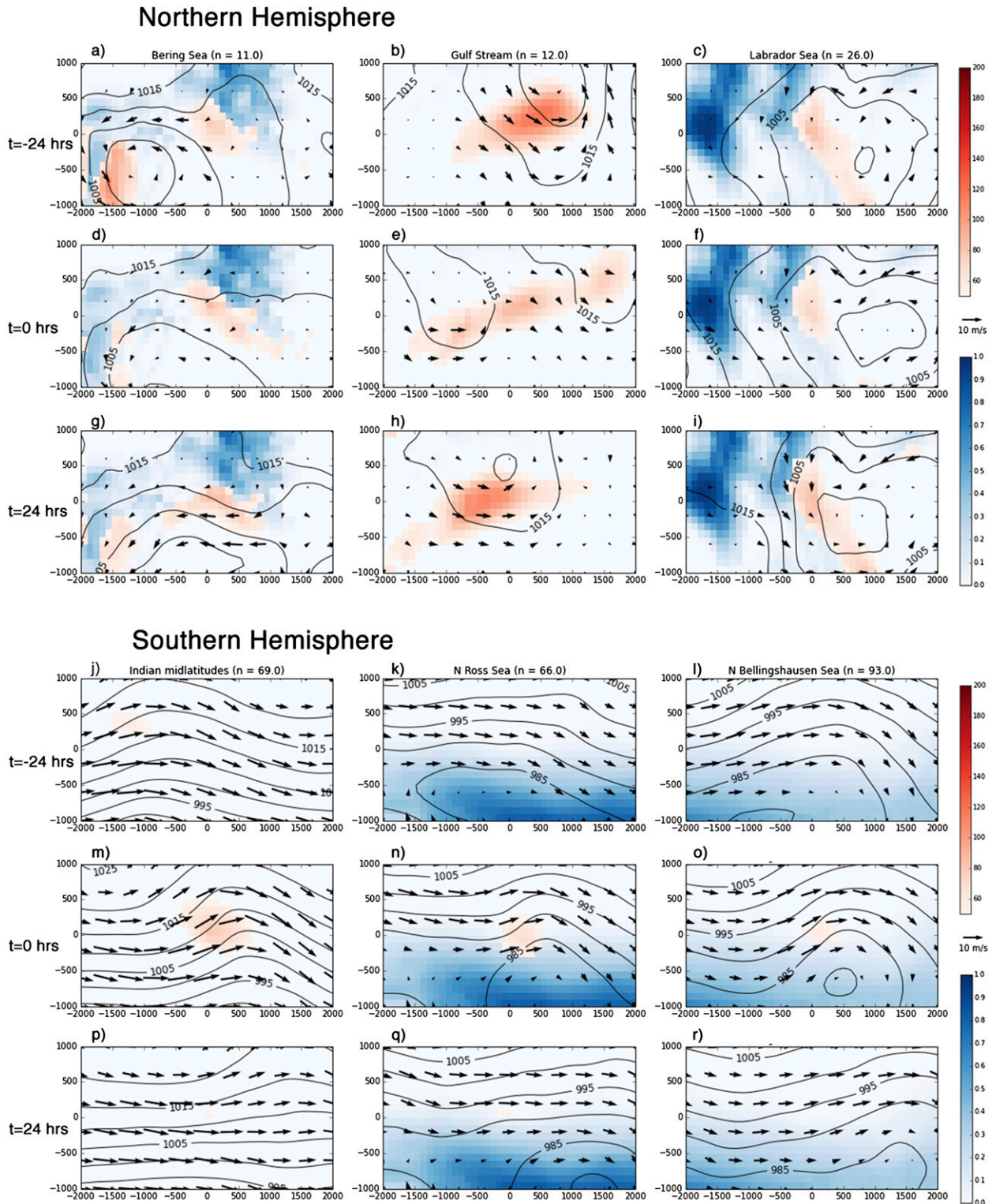
Northern Hemisphere

Southern Hemisphere

FIG. 7. Composite sea level pressure (hPa; contours), 10-m winds (arrows), fractional sea ice cover (blue), and surface SHF (W m^{-2}; red) for weak ($M_{max} \leq 3$ K) MCAO events. NH regions: (a),(d),(g) Bering Sea; (b),(e),(h) Gulf Stream; and (c),(f),(i) Labrador Sea. SH regions: (j),(m),(p) Indian Ocean midlatitudes; (k),(n),(q) Ross Sea; and (l),(o),(r) Bellingshausen Sea. Results are 24 h before the MCAO event in (a)–(c) and (j)–(l), at the event time in (d)–(f) and (m)–(o), and 24 h later in (g)–(i) and (p)–(r). Composites are centered on the location of M_{max}.
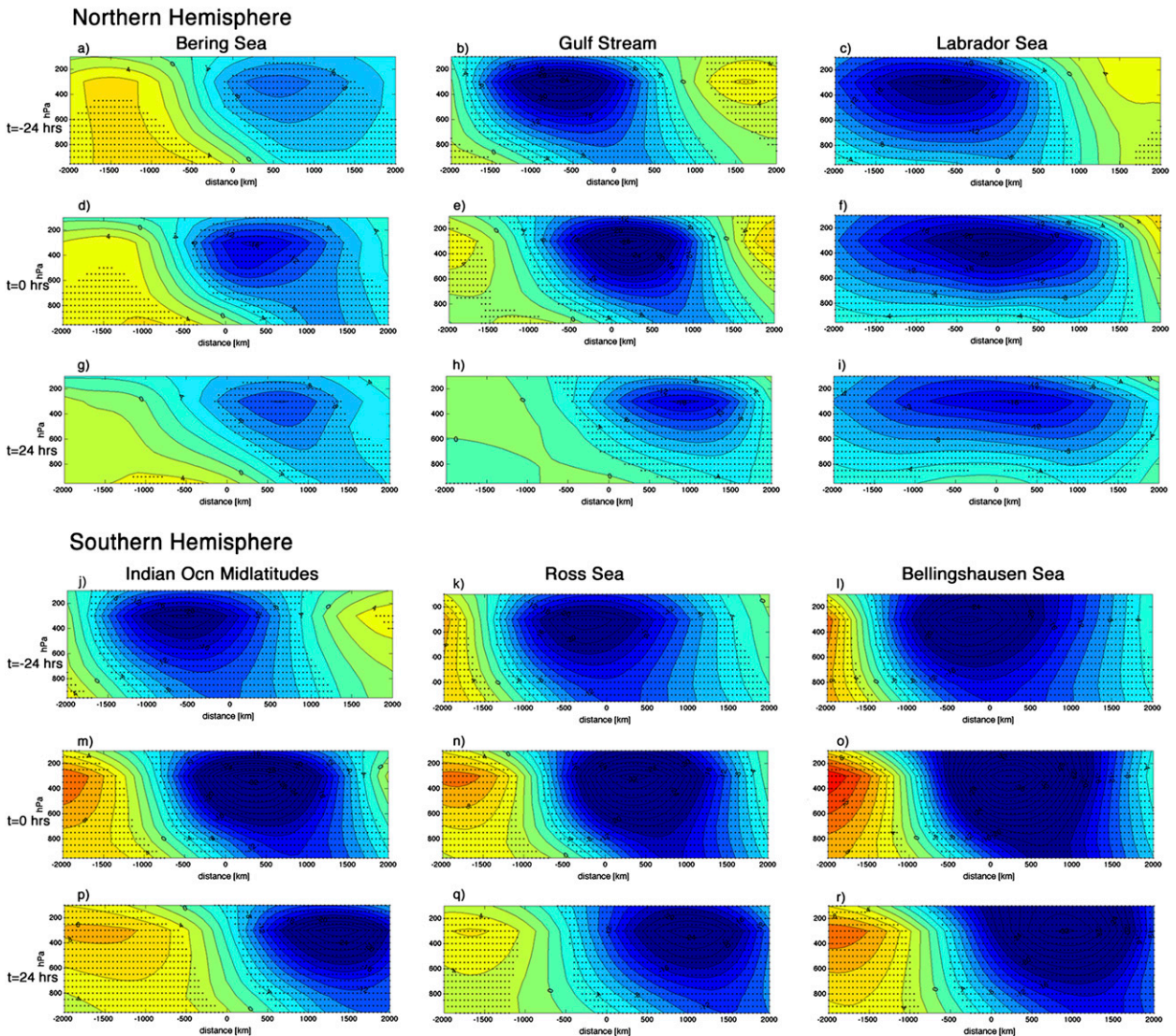
FIG. 8. Composite MCAO event geopotential height anomalies (dam) in cross section along $y = 0$ for the regions shown in Fig. 6. Results are (a)–(c) and (j)–(l) 24 h before the MCAO event, (d)–(f) and (m)–(o) at the event time, and (g)–(i) and (p)–(r) 24 h later. Composites are centered on the location of M_{max}. Stippling indicates areas where anomalies have a <0.05 probability of occurring by chance.

surface low and its decay after the MCAO event. However, in the NH high-latitude regions, both the synoptic-scale flow and the MCAO itself (as shown by the SHF) are more persistent than in other regions.

It is interesting to compare weak and strong MCAO composites for the high-latitude Southern Ocean (i.e., Figs. 6n,o and 7n,o). Although composites are in the same regions and seasons, much more sea ice is shown under the strong events than the weak ones. Although all regions require the availability of cold air masses in order for MCAOs to form, the relationship between sea ice and MCAO frequency and strength is particularly important for the Southern Hemisphere. We will explore this in much more detail in a forthcoming study.

Because weak MCAO events have been shown to occur under a range of synoptic conditions with weak and/or mainly zonal flow on average, for the remainder of this paper we focus on composites of strong MCAO events only.

2) GEOPOTENTIAL HEIGHT

Next we explore the vertical structure of MCAO events. Figure 8 shows geopotential height anomalies in a west–east cross section through the $y = 0$ line in the composites shown in Fig. 6. Anomalies were calculated with respect to the monthly climatology at each grid point. Areas where the anomalies have less than 0.05 probability of occurring by chance are stippled; this

probability was calculated with a two-sided Student's t test, with the number of degrees of freedom equal to the number of events occurring more than 12 h apart.

Consistent with Fig. 6, severe events are associated with a strong upper-level trough that usually exhibits a westward baroclinic tilt, implying that many of these cyclones are still in the growth phase. This is most apparent in the Bering Sea, Gulf Stream, and Indian Ocean regions, while the Ross Sea and Bellingshausen Sea height anomalies are more vertically stacked. However, MCAOs in the Labrador Sea occur under broad upper-level troughs with a zonal extent of 3000–4000 km. The surface cyclone is less apparent in this region because it is to the north of the cross section (Fig. 6f). All of the upper-level troughs deepen over the first 24 h and either decay or maintain strength in the subsequent 24 h. The rapid decay of the surface cyclone in the Gulf Stream MCAOs in the final 24 h in Fig. 6h is also seen in Fig. 8h, but the upper-level anomalies persist.

3) PBL STRUCTURE

Next, we examine similarities and differences in planetary boundary layer (PBL) structure in the composite MCAOs. Figure 9 shows composites of sea level pressure, the difference in horizontal winds between 10 m and 800 hPa ($\mathbf{u}_{800} - \mathbf{u}_{10m}$), and boundary layer height.

The change in wind speed from the surface to 800 hPa is fairly weak, less than $5 \, \mathrm{m \, s^{-1}}$, at the center of the MCAO, but increases in magnitude downstream. It is likely that the surface-driven convection is mixing momentum effectively within the boundary layer near the center of the MCAO. Outside of this region the increase in wind speed ranges from 0 to $10 \, \mathrm{m \, s^{-1}}$.

The ERA-Interim boundary layer height is diagnosed with a dry Richardson number, and so indicates the base of boundary layer clouds rather than their top (von Engeln and Teixeira 2013). The PBL deepens from a few hundred meters to 1–2 km downstream of the MCAO maximum. Boundary layer deepening is driven by surface heating, and the location of the maximum boundary layer depth is downstream of that of the maximum surface heat flux shown in Fig. 6. The overall boundary layer height is greatest at the time of the MCAO event, with fairly rapid reduction in PBL top 24 h later.

Figure 10 shows cross-sectional composites of thermodynamic variables in the lower troposphere for severe events in both hemispheres. In the interest of space, we only show cross sections at the time of the MCAO event and only for two regions per hemisphere. Instead of running from west to east as in Fig. 8, cross sections run along the direction of the 800-hPa winds at the location of M_{max} (the origin of the composites). The locations of the cross sections are shown schematically

as black thick lines in Fig. 6. We composited liquid water potential temperature, $\theta_l = \theta - (L_v/C_p)q_l$ and total water specific humidity, $q_T = q_v + q_l + q_i$, from 1000 to 700 hPa. Here L_v and C_p are the latent heat of vaporization and the heat capacity of dry air, respectively, and q_v, q_l, and q_i are the specific humidity of vapor, liquid water, and ice, respectively.

Although the along-wind cross section is not a perfect trajectory, it depicts the change in boundary layer structure as cold air masses pass over warm water. The NH cross sections qualitatively match the dropsonde measurements of a cold air outbreak case near Svalbard in Hartmann et al. (1997). Upwind of the MCAO maximum, the boundary layer is in a regime of large-scale subsidence with radiative cooling over sea ice; both contribute to a stable boundary layer. As it is advected over warm water, it is heated from below and destabilized. Both surface fluxes and entrainment warm the boundary layer until it evolves into a well-mixed or weakly stable layer downstream. The convective mixing transports potentially warm and relatively moist air upward as the boundary layer deepens downstream of the MCAO maximum. In the lower PBL in the NH cases, this vertically transported warm, moist air is replenished by surface fluxes. In the SH, especially the high-latitude Ross Sea region, the surface fluxes diminish more rapidly along the trajectory and cut off the lower boundary layer from its source of moisture (cf. Figs. 6f and 6n). Figure 10g shows that the near-surface boundary layer therefore begins to dry not far past the MCAO maximum while the overall PBL moisture increases. The lower PBL cooling on the right side of Fig. 10e is likely due to the influence of colder airstreams intersected by the cross section at its northeastern edge.

4. Summary and conclusions

We used an MCAO index to develop a comprehensive climatology of Southern Hemisphere MCAOs, including their extremes and frequency of occurrence, and compare that to a similar climatology of Northern Hemisphere MCAOs. We used this index to define MCAO events and compare the frequency, size and shape, synoptic environment, and PBL structure among composite events for different hemispheres and regions.

Our most important results are as follows:

1) The frequency of occurrence of MCAOs depends on how they are defined. From a gridpoint-by-gridpoint perspective, MCAOs occur most often in Northern Hemisphere winter. But when classified as discrete events, with each counting as a single MCAO regardless of how many grid points it occupies, MCAO frequency of occurrence and seasonality looks

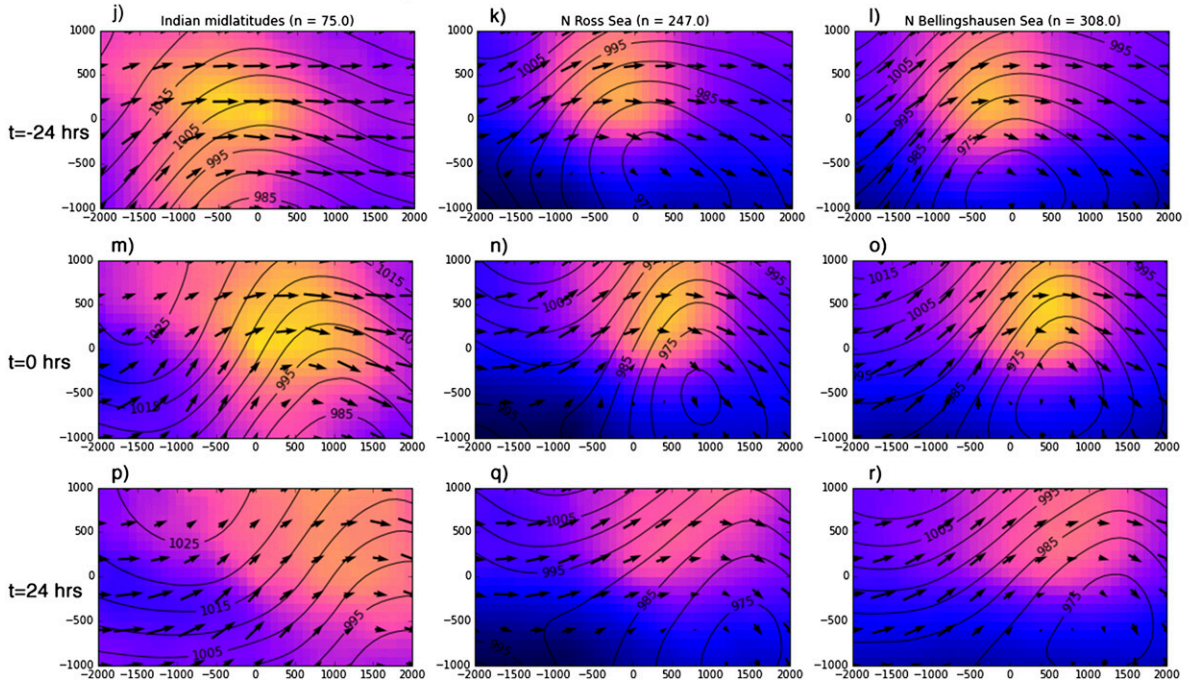## Northern Hemisphere
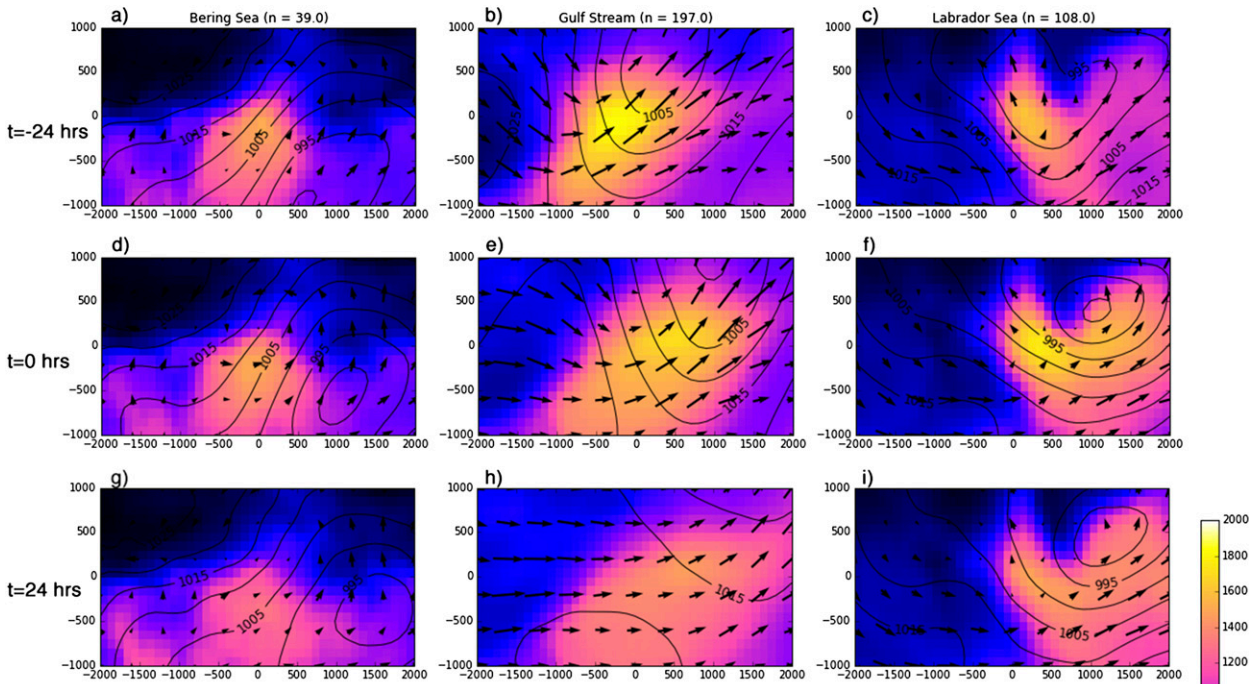
Southern Hemisphere

FIG. 9. Composite sea level pressure (hPa; contours), vertical difference in the 10-m to 800-hPa horizontal winds (m s^{-1}; arrows), and boundary layer height (m; colors) for strong ($M_{max} > 6$ K) MCAO events. NH regions: (a),(d),(g) Bering Sea; (b),(e),(h) Gulf Stream; (c),(f),(i) Labrador Sea. SH regions: (j),(m),(p) Indian Ocean midlatitudes; (k),(n),(q) Ross Sea; and (l),(o),(r) Bellingshausen Sea. Results are 24 h before the MCAO event in (a)–(c) and (j)–(l), at the event time in (d)–(f) and (m)–(o), and 24 h later in (g)–(i) and (p)–(r). Composites are centered on the location of M_{max}.

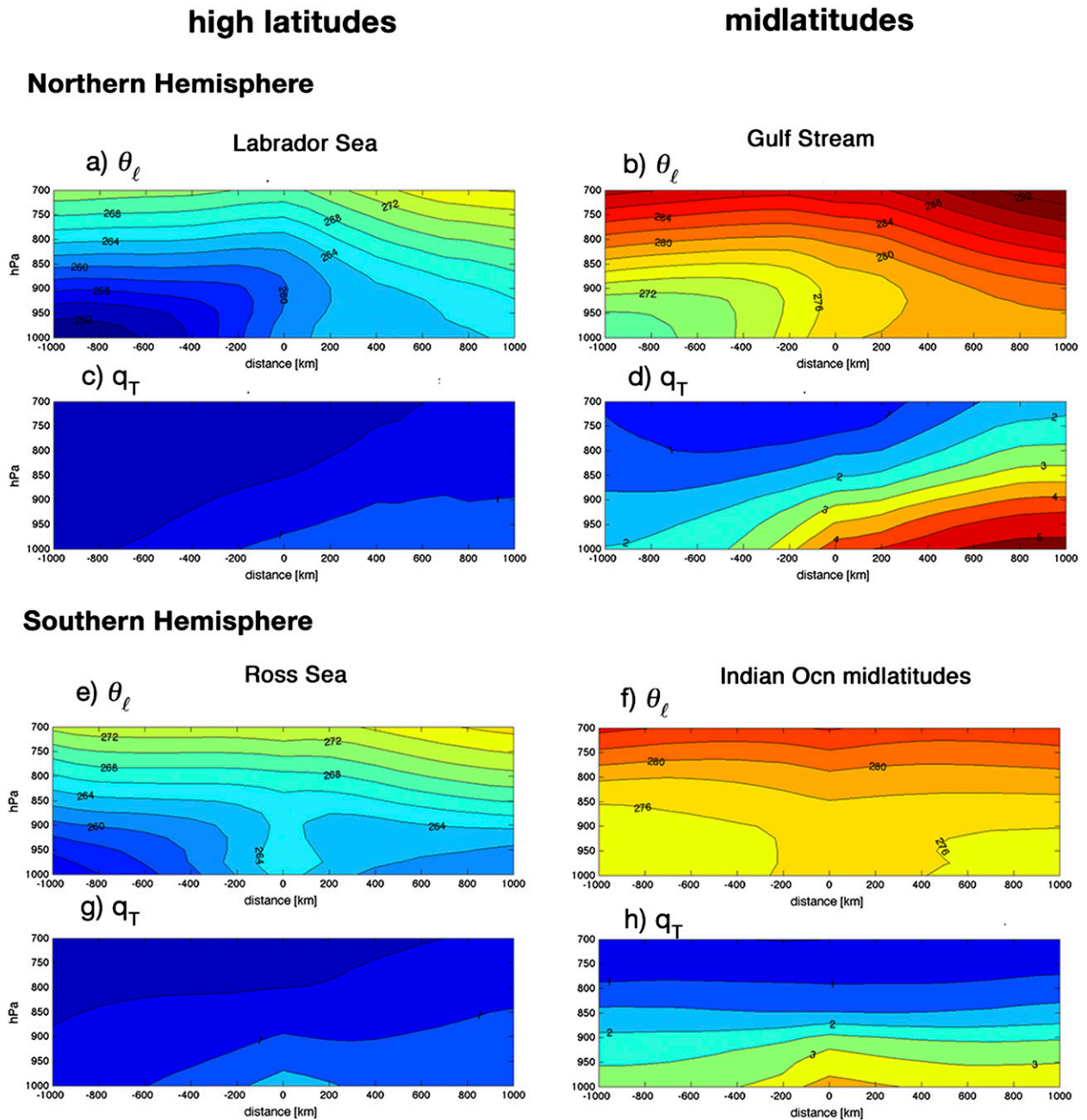## high latitudes

midlatitudes

Northern Hemisphere

FIG. 10. Cross-sectional composites of boundary layer structure in example strong ($M_{max} > 6$ K) MCAO events. The cross section runs from left to right along the direction of the 800-hPa wind at the location of M_{max} (see text and Fig. 6). (a),(b),(e),(f) Liquid water potential temperature (K) and (c),(d),(g),(h) total water specific humidity (g kg^{-1}).

different. They are most frequent in SH autumn, and have only a weak annual cycle in frequency in the SH. The difference occurs because SH warm-season MCAOs are much smaller in scale than their winter counterparts; they, thus, occupy far fewer grid points in ERA-Interim even while discrete events occur with about the same frequency in all seasons. Many MCAOs exist outside of winter, particularly in

shoulder seasons and SH summer, but they are smaller and weaker than their winter counterparts.

2) Strong ($M_{max} > 6$ K) MCAO events have similar synoptic environments and boundary layer structure in both hemispheres. They occur in the cold air sector of extratropical cyclones optimally positioned to advect polar or very cold continental air masses over warm water. The high surface heat fluxes within

MCAOs contribute to the deepening of the boundary layer by 500–1800 m.

3) In the Southern Hemisphere, weak MCAOs $(0 < M_{max} < 3\,K)$ are dynamically somewhat similar to strong MCAOs, albeit with weaker surface lows and a more overall zonal flow. Weak NH events do not have a characteristic synoptic environment, especially at midlatitudes. This is because greater surface skin temperature gradients exist in the NH and occur with a greater range of geometries than in the SH, allowing for a greater range of synoptic environments conducive to the advection of moderately cold air masses. Therefore, the weak end of the MCAO index is somewhat more well suited to SH MCAOs than NH MCAOs.

The cause of the air–sea temperature contrast captured by the MCAO index is different for different regions. In both hemispheres, MCAOs in high-latitude regions are caused by polar air originating over continents or sea ice flowing over open ocean. In the SH midlatitude regions, areas of strong meridional SST gradients create high air–sea temperature contrasts when moderately cold air flows over them. Often this air originated as a stronger MCAO in the higher-latitude regions. It was warmed by surface fluxes, reducing the MCAO index. The MCAO is then reinvigorated when it reaches the strong meridional temperature gradient associated with the Agulhas and Brazil Currents and the Indian subtropical front. This can be seen readily in examination of the supplemental material.

The midlatitude NH MCAO regions are a combination of the two: cold continents provide the very cold air masses while strong SST gradients associated with boundary currents amplify the effect. This is why these regions, particularly the Gulf Stream and Kuroshio, have the strongest MCAOs. Figure 5 shows that all regions outside of these two have fairly similar distributions of MCAO strength regardless of hemisphere.

Figure 6 further shows that, while the details of the synoptic environments most conducive to MCAOs depends strongly on the effects of orography and sea ice distribution, MCAOs are not all that different across hemispheres. The index and methods here prove useful for global analysis and intercomparison. In particular, M can be used to compare the distribution of MCAO strength and frequency, both globally and regionally, between climate models and reanalysis. It may further be used to study and compare features within MCAOs, such as clouds, and for in-depth studies of the dynamics of MCAO development in specific regions.

REFERENCES

Atkinson, B., and J. Wu Zhang, 1996: Mesoscale shallow convection in the atmosphere. *Rev. Geophys.*, **34**, 403–431, doi:10.1029/96RG02623.

Bodas-Salcedo, A., K. D. Williams, P. R. Field, and A. P. Lock, 2012: The surface downwelling solar radiation surplus over the Southern Ocean in the Met Office model: The role of mid-latitude cyclone clouds. *J. Climate*, **25**, 7467–7486, doi:10.1175/JCLI-D-11-00702.1.

——, and Coauthors, 2014: Origins of the solar radiation biases over the Southern Ocean in CFMIP2 models. *J. Climate*, **27**, 41–56, doi:10.1175/JCLI-D-13-00169.1.

Bourassa, M. A., and Coauthors, 2013: High-latitude ocean and sea ice surface fluxes: Challenges for climate research. *Bull. Amer. Meteor. Soc.*, **94**, 403–423, doi:10.1175/BAMS-D-11-00244.1.

Bracegirdle, T. J., and E. W. Kolstad, 2010: Climatology and variability of Southern Hemisphere marine cold-air outbreaks. *Tellus*, **62A**, 202–208, doi:10.1111/j.1600-0870.2009.00431.x.

Brümmer, B., 1996: Boundary-layer modification in wintertime cold-air outbreaks from the Arctic sea ice. *Bound.-Layer Meteor.*, **80**, 109–125, doi:10.1007/BF00119014.

——, 1999: Roll and cell convection in wintertime Arctic cold-air outbreaks. *J. Atmos. Sci.*, **56**, 2613–2636, doi:10.1175/1520-0469(1999)056<2613:RACCIW>2.0.CO;2.

——, and S. Pohlmann, 2000: Wintertime roll and cell convection over Greenland and Barents Sea regions: A climatology. *J. Geophys. Res.*, **105**, 15 559–15 566, doi:10.1029/1999JD900841.

Businger, S., 1985: The synoptic climatology of polar low outbreaks. *Tellus*, **37A**, 419–432, doi:10.1111/j.1600-0870.1985.tb00441.x.

Carleton, A. M., and Y. Song, 1997: Synoptic climatology, and intrahemispheric associations, of cold air mesocyclones in the Australasian sector. *J. Geophys. Res.*, **102**, 13 873–13 887, doi:10.1029/96JD03357.

Chou, S. H., and M. P. Ferguson, 1991: Heat fluxes and roll circulations over the western Gulf Stream during an intense cold-air outbreak. *Bound.-Layer Meteor.*, **55**, 255–281, doi:10.1007/BF00122580.

Condron, A., G. R. Bigg, and I. A. Renfrew, 2008: Modeling the impact of polar mesocyclones on ocean circulation. *J. Geophys. Res.*, **113**, C10005, doi:10.1029/2007JC004599.

Dee, D. P., and Coauthors, 2011: The ERA-Interim reanalysis: Configuration and performance of the data assimilation system. *Quart. J. Roy. Meteor. Soc.*, **137**, 553–597, doi:10.1002/qj.828.

Etling, D., and R. A. Brown, 1993: Roll vortices in the planetary boundary layer: A review. *Bound.-Layer Meteor.*, **65**, 215–248, doi:10.1007/BF00705527.

Field, P. R., R. J. Cotton, K. McBeath, A. P. Lock, S. Webster, and R. P. Allan, 2014: Improving a convection-permitting model simulation of a cold air outbreak. *Quart. J. Roy. Meteor. Soc.*, **140**, 124–138, doi:10.1002/qj.2116.

Hartmann, J., C. Kottmeier, and S. Raasch, 1997: Roll vortices and boundary-layer development during a cold air outbreak. *Bound.-Layer Meteor.*, **84**, 45–65, doi:10.1023/A:1000392931768.

Hein, P. F., and R. A. Brown, 1988: Observations of longitudinal roll vortices during arctic cold air outbreaks over open

water. *Bound.-Layer Meteor.*, **45**, 177–199, doi:10.1007/BF00120822.

Hoskins, B. J., and K. I. Hodges, 2005: A new perspective on Southern Hemisphere storm tracks. *J. Climate*, **18**, 4108–4129, doi:10.1175/JCLI3570.1.

Hwang, Y.-T., and D. M. Frierson, 2013: Link between the double-intertropical convergence zone problem and cloud biases over the southern ocean. *Proc. Natl. Acad. Sci. USA*, **110**, 4935–4940, doi:10.1073/pnas.1213302110.

Isachsen, P. E., M. Drivdal, S. Eastwood, Y. Gusdal, G. Noer, and Ø. Saetra, 2013: Observations of the ocean response to cold air outbreaks and polar lows over the Nordic Seas. *Geophys. Res. Lett.*, **40**, 3667–3671, doi:10.1002/grl.50705.

Kolstad, E. W., 2011: A global climatology of favourable conditions for polar lows. *Quart. J. Roy. Meteor. Soc.*, **137**, 1749–1761, doi:10.1002/qj.888.

——, and T. J. Bracegirdle, 2008: Marine cold-air outbreaks in the future: An assessment of IPCC AR4 model results for the Northern Hemisphere. *Climate Dyn.*, **30**, 871–885, doi:10.1007/s00382-007-0331-0.

——, ——, and I. A. Seierstad, 2009: Marine cold-air outbreaks in the North Atlantic: Temporal distribution and associations with large-scale atmospheric circulation. *Climate Dyn.*, **33**, 187–197, doi:10.1007/s00382-008-0431-5.

Müller, G., and A. Chlond, 1996: Three-dimensional numerical study of cell broadening during cold-air outbreaks. *Bound.-Layer Meteor.*, **81**, 289–323, doi:10.1007/BF02430333.

Papritz, L., S. Pfahl, H. Sodemann, and H. Wernli, 2015: A climatology of cold air outbreaks and their impact on air–sea heat fluxes in the high-latitude South Pacific. *J. Climate*, **28**, 342–364, doi:10.1175/JCLI-D-14-00482.1.

Parish, T. R., and D. H. Bromwich, 2007: Reexamination of the near-surface airflow over the Antarctic continent and implications on atmospheric circulations at high southern latitudes. *Mon. Wea. Rev.*, **135**, 1961–1973, doi:10.1175/MWR3374.1.

Rasmussen, E. A., and J. Turner, 2003: *Polar Lows: Mesoscale Weather Systems in the Polar Regions.* Cambridge University Press, 612 pp.

Renfrew, I. A., and G. W. K. Moore, 1999: An extreme cold-air outbreak over the Labrador Sea: Roll vortices and air–sea interaction. *Mon. Wea. Rev.*, **127**, 2379–2394, doi:10.1175/1520-0493(1999)127<2379:AECAOO>2.0.CO;2.

Schröter, M., S. Raasch, and H. Jansen, 2005: Cell broadening revisited: Results from high-resolution large-eddy simulations of cold air outbreaks. *J. Atmos. Sci.*, **62**, 2023–2032, doi:10.1175/JAS3451.1.

Simmonds, I., K. Keay, and E.-P. Lim, 2003: Synoptic activity in the seas around Antarctica. *Mon. Wea. Rev.*, **131**, 272–288, doi:10.1175/1520-0493(2003)131<0272:SAITSA>2.0.CO;2.

Simpkins, G. R., L. M. Ciasto, D. W. Thompson, and M. H. England, 2012: Seasonal relationships between large-scale climate variability and Antarctic sea ice concentration. *J. Climate*, **25**, 5451–5469, doi:10.1175/JCLI-D-11-00367.1.

Stage, S. A., and J. A. Businger, 1981: A model for entrainment into a cloud-topped marine boundary layer. Part I: Model description and application to a cold-air outbreak episode. *J. Atmos. Sci.*, **38**, 2213–2229, doi:10.1175/1520-0469(1981)038<2213:AMFEIA>2.0.CO;2.

Trenberth, K. E., 1991: Storm tracks in the Southern Hemisphere. *J. Atmos. Sci.*, **48**, 2159–2178, doi:10.1175/1520-0469(1991)048<2159:STITSH>2.0.CO;2.

——, and J. T. Fasullo, 2010: Simulation of present-day and twenty-first-century energy budgets of the Southern Oceans. *J. Climate*, **23**, 440–454, doi:10.1175/2009JCLI3152.1.

Våge, K., T. Spengler, H. C. Davies, and R. S. Pickart, 2009: Multi-event analysis of the westerly Greenland tip jet based upon 45 winters in ERA-40. *Quart. J. Roy. Meteor. Soc.*, **135**, 1999–2011, doi:10.1002/qj.488.

von Engeln, A., and J. Teixeira, 2013: A planetary boundary layer height climatology derived from ECMWF reanalysis data. *J. Climate*, **26**, 6575–6590, doi:10.1175/JCLI-D-12-00385.1.

Williams, K. D., and Coauthors, 2013: The Transpose-AMIP II Experiment and its application to the understanding of Southern Ocean cloud biases in climate models. *J. Climate*, **26**, 3258–3274, doi:10.1175/JCLI-D-12-00429.1.